Universal features of rigidity transitions in vertex models for biological tissues

Ojan Khatib Damavandi[1], **Elizabeth Lawson-Keister**[1], **M. Lisa Manning**[1*]

***For correspondence:** mmanning@syr.edu (MLM)

[1]Department of Physics and BioInspired Institute, Syracuse University, Syracuse, NY 13244

Abstract For confluent or nearly confluent tissues, simulations and analyses of simple vertex models – where the cell shape is defined as a network of edges and vertices – have proven useful for making predictions about mechanics and collective behavior, including rigidity transitions. Scientists have developed many versions of vertex models with different assumptions. Here we investigate a set of vertex models which differ in the functional form that describes how energy depends on the vertex positions. We analyze whether such models have a well-defined shear modulus in the limit of zero applied strain rate, and if so how that modulus depends on model parameters. We identify a class of models with a well-defined shear modulus, and demonstrate that these models do exhibit a cross-over from a soft or floppy regime to a stiff regime as a function of a single control parameter, similar to the standard vertex model. Moreover, and perhaps more surprisingly, the rigidity crossover is associated with a crossover in the observed cell shape index (the ratio of the cell perimeter to the square root of the cell area), just as in the standard vertex model, even though the control parameters are different. This suggests that there may be a broad class of vertex models with these universal features, and helps to explain why vertex models are able to robustly predict these features in experiments.

Introduction

In biological processes ranging from embryonic development to cancer metastasis, recent work has emphasized that the collective behavior of cells plays an important role ***Angelini et al.*** (***2011***); ***Ilina et al.*** (***2020***); ***Noll et al.*** (***2017***). It is becoming increasingly clear that many of these animal tissues undergo a fluid-solid transition which is important for their function ***Mongera et al.*** (***2018***); ***Park et al.*** (***2015***); ***Wang et al.*** (***2020***); tissues fluidize in order to allow large-scale deformation and flows and then solidify to maintain functional shapes and support shear stresses.

Theoretical and computational work in concert with experimental observations have identified several mechanisms ***Lawson-Keister and Manning*** (***2021***) that can generate fluid-solid transitions tissues, including an increase in cell density to increase the number of contacts and generate percolating rigid cluster ***Mongera et al.*** (***2018***); ***Petridou et al.*** (***2021***), a tension-driven rigidity transition in the vertex model ***Farhadifar et al.*** (***2007***); ***Bi et al.*** (***2015***), change in active fluctuations ***Devany et al.*** (***2021***).

Of course, quantifying the onset fluid-solid transitions in disordered materials is a non-trivial problem in and of itself, so these works have also had to develop heuristic tools to do so. The obvious technique from materials science is the shear modulus, which is defined as the linear response of the system to an applied shear strain in the limit of infinitely slow driving, a definition

that works best at zero temperature when there are no competing timescales ***Ashcroft and Mermin*** (***1976***). In glassy systems at finite temperature, there can be quite large competing timescales, and so in practice experiments on glassy materials define a material to be solid when its measured viscosity exceeds a specified threshold ***Weeks et al.*** (***2000***). Similar methods in simulations of active glassy matter place a threshold on the measured diffusion constant ***Bi et al.*** (***2016***) or self-overlap function ***Paoluzzi et al.*** (***2021***). A challenge is that many of these dynamic definitions depend on the choice of threshold and details of implementation.

Despite these challenges, it is clear that coarse-grained models have made successful predictions for fluid-to-solid transitions in tissues. Particle-based models have made accurate quantitative predictions for the relationship between cell density and network connectivity and tissue fluidity in the developing zebrafish embryo ***Mongera et al.*** (***2018***); ***Petridou et al.*** (***2021***), and vertex models have made accurate quantitative predictions for the relationship between cell shape and tissue fluidity/remodeling in human bronchial epithelial tissues ***Park et al.*** (***2015***), fruit fly embryos ***Wang et al.*** (***2020***) and MDCK monolayers ***Devany et al.*** (***2019***).

In this work, we focus on the vertex models, which assume that a confluent epithelial monolayer with no gaps or overlaps between cells can be described as a network of edges and vertices ***Nagai and Honda*** (***2001***); ***Farhadifar et al.*** (***2007***); ***Hufnagel et al.*** (***2007***). In a standard version of the model, the energy functional that describes the tissue is written as a sum of two terms: a quadratic penalty on the cross-sectional area and cross-sectional perimeter when those quantities deviate from their target values. These terms naturally arise when considering volume incompressibility, cortical tension and adhesion, and active contractility in epithelial monolayers ***Farhadifar et al.*** (***2007***).

Much of the work on vertex models has focused on 2D systems, as epithelial monolayers occur regularly in development and disease processes and the experimental data is fairly straightforward to compare to models. Although some work has suggested that similar rigidity transitions occur in 3D tissues as well ***Merkel and Manning*** (***2018***); ***Mongera et al.*** (***2018***); ***Grosser et al.*** (***2021***), for simplicity and to make clear connections with previous literature, we also focus here on 2D models.

While the tension-driven rigidity transition appears to be a quantitatively predictive theory for several experimental systems (mainly in epithelia), the simple vertex model that has been used to study features of the rigidity transition is in some ways clearly too simple. It does not include many features that are obviously relevant for real biological tissues. Therefore, an open question remains: why is it predictive at all?

One possible answer to this question is that there is a class of more complex models that all exhibit an underlying rigidity transition with universal features. To understand whether something like this is possible, it is useful to examine variations of vertex models that have recently been proposed in the literature.

One set of vertex model variations have altered the initial conditions or the dynamics of the vertex model to add specific biologically relevant details, and studied the resulting rigidity transition. One study investigated the effect of rosette formation ***Yan and Bi*** (***2019***), finding that an increasing number of rosettes further rigidifies a tissue. A related series of studies investigated vertex models with so-called "T1 delay times", where it is assumed that molecular-scale processes could impede individual cell-rearrangements over a characteristic timescale ***Erdemci-Tandogan and Manning*** (***2021***); ***Das et al.*** (***2021***). In those models, delay times could also enhance the rigidity of tissues and also generate cellular streaming patterns consistent with experimental observations. Another set of studies investigated how heterogeneities in cell stiffnesses affect vertex models, finding that rigidity percolation of a sub-population of stiff cells could be used to explain the onset of rigidity in that case ***Li et al.*** (***2019***).

A second set of works instead study vertex model variations that are more drastic – fundamentally altering the vertex energy functional itself by adding different or dynamical degrees of freedom. One such work is the active foam model developed by Kim et al ***Kim et al.*** (***2020***), which removes the second-order term that penalizes deviations from a target perimeter. Instead, there

is only a linear penalty for variations to the perimeter, similar to the role surface tension plays in foams. Another variation is replacing the second-order term for the perimeter with a second-order term penalizing deviations of each individual edge length from a target value, generating a system that is reminiscent of a spring network, albeit still with constraints on cell areas. An even more realistic variation is to allow the edges to have additional degrees of freedom and dynamics that are described by additional differential equations. In work by Staddon and collaborators ***Staddon et al.*** (***2019***), edges are mechanosensitive springs that possess rest-lengths that can change depending on the tension and strain across the edge. In work by Noll et al ***Noll et al.*** (***2017***), edges are springs with rest-lengths that are governed by myosin dynamics, which is, in turn, mechanosensitive and governed by tension on the edges.

An obvious question, then, is how this more drastic (and realistic) set of perturbations to vertex models affects tissue fluidity and the fluid-to-solid transition. Is there still a rigidity transition in such systems? If so, does the transition exhibit similar features to the one seen in standard vertex models? If there are universal features in a broad class of vertex models, this could help explain why such simple models are quantitatively predictive in experiments. It is also useful to examine non-universal features, as differences could help point the way to experiments that can distinguish between models.

Here, we analyze the onset of rigidity in a set of six vertex models: the standard vertex model and five others where the energy functional is fundamentally altered. We focus on the quasi-static limit of such models so that shear modulus in the limit of infinitely slow driving is well-defined, and quantify whether each model exhibits a crossover from floppy to rigid behavior, which model parameters control the behavior, and whether observable structural features are associated with the crossover.

Models and Methods

We first develop a framework for comparing different vertex models to one another. The change in free energy of a vertex model can be written generally as

$$\mathrm{d}E(\{\mathbf{r}_i\}) = \mathrm{d}E(\{A_\alpha\}, \{l_{ij}\}) = \sum_\alpha \pi_\alpha \mathrm{d}A_\alpha + \sum_{\langle i,j \rangle} T_{ij} \mathrm{d}l_{ij} \tag{1}$$

where $\{\mathbf{r}_i\}$ is the set of vertex coordinates, $\{A_\alpha\}$ is the area of cell α, $\{l_{ij}\}$ is the length of the edge between vertices i and j, and $T_{ij} = \frac{\partial E}{\partial l_{ij}}$ is the tension on the edge between vertices i and j. Pressure, π_α, generally depends linearly on how far cell areas are from their preferred area A_0. The choice of the form of edge tensions can lead to different vertex models with potentially different properties.

As this work focuses on rigidity transitions in vertex models in the limit of zero fluctuations, we use the shear modulus as the metric for rigidity, as it is zero in a floppy or fluid-like system and non-zero in a rigid system, except under special circumstances ***Damavandi et al.*** (***2022a***). The shear modulus G is defined as the second derivative of the energy E with respect to applied shear strain γ, or equivalently the first derivative of the shear stress σ with respect to γ:

$$G = \frac{1}{V}\frac{d^2E}{d\gamma^2} = \frac{d\sigma}{d\gamma}, \tag{2}$$

In practice, we compute G in our simulations using the Hessian matrix of second derivatives of the energy with respect to vertex displacements ***Merkel and Manning*** (***2018***):

$$G = \frac{1}{N_c}\left(\frac{\partial^2 E}{\partial \gamma^2} - \sum_m \frac{1}{\omega_m^2}\left[\sum_{j,\alpha} \frac{\partial^2 e}{\partial \gamma \partial r_j^\alpha} u_{j\alpha}^m\right]^2\right), \tag{3}$$

where ω_m^2 are the non zero eigenvalues of the Hessian $D_{j\alpha,k\beta}$, and $u_{j\alpha}^m$ are the corresponding normalized eigenvectors:

$$D_{j\alpha,k\beta} = \sum_m \omega_m^2 u_{j\alpha}^m u_{k\beta}^m. \tag{4}$$

Vertex model

One of the most widely used models, introduced by Farhadifar et al ***Farhadifar et al.*** (***2007***) and which we simply call the vertex model, assumes that tension on an edge of cell α is proportional to $P_\alpha - P_0$, where P_0 is the cell's preferred perimeter. For a system that follows this vertex model, the energy integrated from Eq. 1, up to a constant, is

$$E = \sum_\alpha \left[K_A(A_\alpha - A_0)^2 + K_P(P_\alpha - P_0)^2\right] \tag{5}$$

This equation can be non-dimensionalized, identifying two dimensionless parameters, the dimensionless ratio between the area and perimeter moduli $K_P/(K_A A_0)$, and the cell target shape index $p_0 = P_0/\sqrt{A_0}$.

As most of the previous work to understand the rigidity transition in this class of models has focused on the standard vertex model, we briefly highlight what is known. First, the seminal work by Farhardifar et al ***Farhadifar et al.*** (***2007***) demonstrated that there were two ground states of this model – a rigid ordered network and a soft disordered network. Bi et al ***Bi et al.*** (***2015***) studied disordered metastable states of the network and found that energy barriers to cellular rearrangements, quantified by statistics of shrinking edges, disappeared above a critical value of the cell target shape index $p_0 = p_0^* \sim 3.81$. This suggests that the standard vertex model exhibits a floppy-to-rigid transition as p_0 is decreased below a critical value. Quantifying the shear modulus near the transition is quite difficult due to the nearly flat energy landscape, but some of us demonstrated that it, too, disappears in disordered systems for $p_0 > p_0^*$ ***Merkel and Manning*** (***2018***).

Interestingly, in ordered ground states of the model, there is a distinction between the onset of rigidity determined by the shear modulus (which occurs at the shape index of a regular hexagon, $p_0 \sim 3.72$), and when energy barriers disappear (at $p_0 = p_0^* \sim 3.81$). This suggests that there must be non-analytic cusps in the potential energy landscape ***Sussman and Merkel*** (***2018***); ***Popović et al.*** (***2021***) and that there may be significant differences between the linear (zero strain rate, infinitesimal strain) and nonlinear (finite strain rate, finite strain) rheology of vertex models, which have recently been studied in 2D ***Duclut et al.*** (***2021***); ***Basan et al.*** (***2011***); ***Popović et al.*** (***2021***) and 3D ***Sanematsu et al.*** (***2021***).

Recent studies have also focused on understanding the underlying mechanism that drives the vertex model rigidity transition, as it does not follow a simple Maxwell constraint counting argument ***Maxwell*** (***1864***); ***Sussman and Merkel*** (***2018***). A few studies have demonstrated that a geometric incompatibility between the lengthscale imposed by the target shape index and the cell area (or equivalently, the shape imposed by the boundary conditions) drives the transition ***Merkel et al.*** (***2019***); ***Moshe et al.*** (***2018***). Most recently, we and collaborators have demonstrated that second-order rigidity (penalties that arise only to second order in the constrains) and not first-order rigidity (another name for Maxwell constraint counting) drives the rigidity transition in vertex models***Damavandi et al.*** (***2022a***,b).

Confluent active foam model

As highlighted in the introduction, recent work by Kim et al ***Kim et al.*** (***2020***) simulated deformable, adhesive particles and demonstrated that there was an interesting crossover from a particle-like jammed system with holes between cells to an epithelial-like rigid material where cells tiled all space. Importantly, this work used a different energy functional than the vertex model discussed above. Called an "active foam" model, the authors did not include a restoring force on the perimeter (i.e. a term proportional to P^2), and instead assumed that the tension on the edges is simply a constant for all edges, $T_{ij} = \Lambda$. In this work we study the confluent limit of the active foam model, where the density is sufficiently high to ensure that the cells tile all space with no gaps.

This constant tension leads to a simple form of the energy functional:

$$E = \sum_{\alpha} K_A (A_\alpha - A_0)^2 + \sum_{\langle i,j \rangle} \Lambda\, l_{ij} \tag{6}$$

$$= \sum_{\alpha} \left[K_A (A_\alpha - A_0)^2 + \Lambda_P\, P_\alpha \right], \tag{7}$$

where $\Lambda_P = \Lambda/2$.

Previous work by Farhardifar et al and Staple et al ***Farhadifar et al.*** (***2007***); ***Staple et al.*** (***2010***) studied this vertex energy for ordered states in a confluent model in the limit that Λ is greater than zero and demonstrated that the system is always rigid. Below, we study the stability of the model when the line tension Λ is zero or negative.

We note that other works explore related changes to the second-order perimeter term of the energy functional. For example, recent work by Latorre et al ***Latorre et al.*** (***2018***) investigates a vertex-like model where the second-order restoring term for the perimeter depends on the cell area/volume, so that as the cell area increases the perimeter restoring force decreases. The authors show that such a model, which acts like the active foam model in the limit of large cell size, generates an instability that reproduces many features of cell expansion in epithelial domes.

Spring Edge Model

In some epithelial systems, it may be that individual cell interfaces behave as if they are elastic, so that there is a restoring force as the length of that edge shrinks. Such a model might be appropriate for plant cells or animal cells with interstitial ECM and is also sometimes chosen for mathematical convenience ***Sadhukhan and Nandi*** (***2021***).

We assume that each edge is a spring with rest (preferred) length l_0. Then, assuming Hooke's law for the tensions $T_{ij} = 2K_l(l_{ij} - l_0)$, and integrating Eq. 1 yields

$$E = \sum_{\alpha} K_A (A_\alpha - A_0)^2 + \sum_{\langle i,j \rangle} K_l (l_{ij} - l_0)^2 \tag{8}$$

In practice, we simulate the following equivalent expression:

$$E = \sum_{\alpha} \left[K_A (A_\alpha - A_0)^2 + \sum_{\langle i,j \rangle} K_P (l_{ij} - l_0)^2 \right] \tag{9}$$

where $K_P = K_l/2$ because each edge is counted twice in Eq. 9.

Active Spring Model

This model developed by Staddon et al ***Staddon et al.*** (***2019***) can be thought of as an extension of the spring edge model where spring rest lengths dynamically change to relax the tension. This model is intended to capture active turnover of the actomyosin bundles that give the edges their contractility, replacing strained elements with unstrained ones. It, therefore, posits that the rest length l^0_{ij} dynamically changes in order to reduce the tension on the edge. It further assumes that only strains above a certain threshold trigger the rest length dynamics, resulting in the following equation of motion:

$$\frac{\mathrm{d}l^0_{ij}}{\mathrm{d}t} = \begin{cases} k_l (l_{ij} - l^0_{ij}) & \text{if } |\epsilon_{ij}| > \epsilon_c \\ 0 & \text{otherwise} \end{cases} \tag{10}$$

where $\epsilon_{ij} = (l_{ij} - l^0_{ij})/l^0_{ij}$.

If $\epsilon_c = 0$, the dynamics will have a completely viscoelastic behavior. This can be seen by taking the time derivative of tension and using Eq. 10: $\dot{T}_{ij} = 2K_l(\dot{l}_{ij} - \dot{l}^0_{ij}) = 2K_l \dot{l}_{ij} - k_l T_{ij}$ or $2K_l \dot{l}_{ij} = \dot{T}_{ij} + T_{ij}/\tau_l$, which is simply the Maxwell model of viscoelasticity, with $\tau_l = 1/k_l$, the remodeling timescale. The system is expected to fully relax edge tensions at long times. This purely viscoelastic model with $\epsilon_c = 0$ was previously studied in a separate manuscript ***Clément et al.*** (***2017***), and the functional

form was justified with fits to experimental data during germband extension in the Drosophila embryo. A nonzero ϵ_c means that there can be residual tensions in the network.

We note that Staddon et al. define the tension and energy in terms of strain ϵ_{ij}. However, to be consistent in our definition of tension, we instead define everything in terms of l_{ij}. We expect that qualitatively our results will be similar as the structure of the system at its dynamical steady state, which we discuss below, is the same between these two versions.

Tension Remodeling Model

Staddon et al. ***Staddon et al.*** (***2019***) also define a second "tension remodeling" model that is more consistent with their experimental observations. Specifically, the active tension model is not consistent with the observation that edges can lose memory of their rest length. To generate this feature, the tension remodeling model posits that tension is constant unless strain on an edge reaches a critical value, triggering remodeling of the tension. This can be understood as an extension of the active foam model, where tensions are always constant. They propose the following equation of motion for the tension T_{ij}:

$$\frac{\mathrm{d}T_{ij}}{\mathrm{d}t} = \begin{cases} -k_e(l_{ij} - l_{ij}^0) & \text{if } \epsilon_{ij} > \epsilon_c \\ 0 & \text{if } -\epsilon_c \leq \epsilon_{ij} \leq \epsilon_c \\ -k_c(l_{ij} - l_{ij}^0) & \text{if } \epsilon_{ij} < -\epsilon_c \end{cases} \tag{11}$$

where k_e and k_c are the rates of remodeling under edge extension and compression.

They further postulate that the rest length remodels until the edge is equilibrated:

$$\frac{\mathrm{d}l_{ij}^0}{\mathrm{d}t} = k_l(l_{ij} - l_{ij}^0). \tag{12}$$

To gain an intuition for this model, first, consider the case where an edge exhibits a strain $\epsilon_{ij} < -\epsilon_c$. Then the edge is under compression, and the tension will start to increase (e.g. the edge will become more contractile). Simultaneously, the rest length will shorten and relax the tension until the edge equilibrates at its (shorter) rest length. A similar argument holds in the actively extensile case $\epsilon_{ij} > \epsilon_c$.

If instead, the strain is within the nonactive regime for the tension dynamics, even though the rest length continues to change until it matches the actual edge length, the tension remains constant and the force on each vertex is thus fixed, so the vertex positions and edge lengths do not change.

Taken together, this suggests that in all cases the rest length is fixed by the edge length determined by the tension. The energy of this model thus is effectively the foam model, Eq. 7 with $\Lambda \to T_{ij}$. If we fix the areas, the force on vertex i is $\mathbf{F}_i = \sum_{\{j\}_i} \mathbf{T}_{ij}$.

Active Tension Network

A model introduced by Noll et al ***Noll et al.*** (***2017***) adds an extra layer of complexity to the tension dynamics by modeling myosin recruitment. The model includes three dynamical processes: 1) vertex dynamics given by energy minimization of Eq. 1, 2) rest length dynamics, and 3) myosin recruitment due to mechanical feedback from the strain at edges.

For their analytics, Noll et al. assume that pressure differences between cells are negligible and thus vertex dynamics are effectively driven by the tension network. With this assumption, the overdamped vertex dynamics (with mobility μ) is given by

$$\frac{\mathrm{d}\mathbf{r}_i}{\mathrm{d}t} = -\mu \sum_{\{j\}_i} \mathbf{T}_{ij}. \tag{13}$$

Additionally, it is assumed that each edge acts like an active spring with dynamically changing rest length. Then, $T_{ij} = 2K_l(l_{ij} - l_{ij}^0)$ as in the spring-edge model and active spring model, and the energy is given by Eq. 8.

However, unlike the spring dynamics in Eq 10, it is assumed that the fixed point of the differential equation is not at zero strain but rather is achieved when tension on the edge is balanced by the myosin recruited on the edge m_{ij}. In this case, the rest length dynamics is given by

$$\frac{1}{l_{ij}^0}\frac{\mathrm{d}l_{ij}^0}{\mathrm{d}t} = \tau_l^{-1} W\left(\frac{T_{ij}}{m_{ij}}\right). \tag{14}$$

$W(x)$ is called the myosin walking kernel, which has the following properties: $W(1) = 0$, $W'(1) = 1$ and the slope of W approaches zero near $x = 0$ and for $x \gg 1$. This means that the fixed point of Eq. 14 is at $T_{ij}^* = m_{ij}^*$. Noll et al. do not consider the $T_{ij} < 0$ regime, as they are interested in near-equilibrium behavior where $T_{ij} > 0$ due to force balance at each vertex. Linearizing near the steady state gives

$$\frac{1}{l_{ij}^0}\frac{\mathrm{d}l_{ij}^0}{\mathrm{d}t} = \tau_l^{-1}\frac{T_{ij} - m_{ij}}{m_{ij}}. \tag{15}$$

Next, they introduce myosin dynamics. If the myosin field was constant in time, Eq. 15 along with $T_{ij} = 2K_l(l_{ij} - l_{ij}^0)$ would describe a viscoelastic behavior for the edge length l_{ij} driven by a shifted (residual) tension $T_{ij} - m_{ij}$, which would be similar to active spring model with $\epsilon_c = 0$. But since mechanical equilibrium specifies a unique set of tensions, this would mean myosin levels could not be independently prescribed. This is in contrast to experimental observations, as myosin levels have been shown to be dynamic and respond to mechanical cues.

Instead, the authors introduce a simple version of myosin activity that ensures mechanical stability, namely that myosin is involved in a direct mechanical feedback from the edge strain,

$$\frac{1}{m_{ij}}\frac{\mathrm{d}m_{ij}}{\mathrm{d}t} = \alpha\frac{1}{l_{ij}^0}\frac{\mathrm{d}l_{ij}^0}{\mathrm{d}t} = \alpha\tau_l^{-1}\frac{T_{ij} - m_{ij}}{m_{ij}}, \tag{16}$$

where the second equality holds near equilibrium.

Results

Using the systematic descriptions of six different versions of vertex models developed in the previous section, we proceed to investigate their stability and rigidity. Our goal is to understand whether they exhibit a rigidity transition similar to the one previously identified in the standard vertex model.

Confluent Active Foam Model

We seek to quantify the stability of the confluent active foam model as a function of the interfacial tension parameter, Λ, which exactly follows the analysis of Staple et al ***Staple et al.*** (***2010***) for the full standard vertex model, except that here we drop the p^2 term. First, we nondimensionalize Eq. 7 for a single cell to get $e = (a-1)^2 + \bar{\Lambda}p$ where $e = E_\alpha/(K_A A_0^2)$, $a = A_\alpha/A_0$, $\bar{\Lambda} = \Lambda/(K_A A_0^{3/2})$ and $p = P_\alpha/\sqrt{A_0}$. To look for energy minima, we scale each edge of the polygon by $\chi = 1 + \delta$: $e \to e' = (\chi^2 a - 1)^2 + \bar{\Lambda}\chi p$ and require $\partial e'/\partial\chi|_{\chi=1} = 0$. We find

$$4a(a-1) + \bar{\Lambda}p = 0 \tag{17}$$

Two trivial solutions are i) $a = 0,\ p = 0$ corresponding to a collapsed polygon, and ii) $a = 1,\ p = 0$, which is not possible to achieve, suggesting that the polygons are frustrated at the energy minima. A nontrivial solution occurs when $a < 1$ (otherwise $\partial e'/\partial\chi|_{\chi=1} > 0$).

Looking at $\partial e/\partial p|_a = \bar{\Lambda}$, we see that for $\bar{\Lambda} < 0$, the energy can be reduced by increasing p, which makes the polygon unstable to shear. For $\bar{\Lambda} > 0$ to reduce energy we need to reduce p as well, suggesting that a regular polygon is the solution.

For a regular polygon, we write $a = cp^2$ with $c = \cot(\pi/n)/4n$ and n the number of edges. Then we can rewrite $e(p) = (cp^2 - 1)^2 + \bar{\Lambda}p$ and look for the solution to $\mathrm{d}e/\mathrm{d}p = 0$: $4c^2p^3 - 4cp + \bar{\Lambda} = 0$.

Additionally, we require the polygons to have $p > 0$ (not collapsed): $(cp^2 - 1)^2 + \bar{\Lambda} > 1$. This suggests that there is a range of $\bar{\Lambda}$ that supports a stable (rigid) polygon:

$$0 \leq \bar{\Lambda} \leq \bar{\Lambda}_c = \frac{2}{c}(\frac{2c}{3})^{\frac{3}{2}} \tag{18}$$

This range is exact only for regular polygons, so in simulations of disordered cellular tilings, we expect that the observed transition point $\bar{\Lambda}_c$ deviates from this ordered prediction. This is indeed what we find; in disordered vertex model simulations some cells collapse for Λ greater than a threshold value (shown in panel c of Fig 1), while for $\Lambda < 0$ the simulation is unstable since there is no restoring force and the energy can keep decreasing for larger and larger perimeters. In this case, vertices cross into neighboring cells and the model becomes unphysical, as illustrated in Fig 1(a).

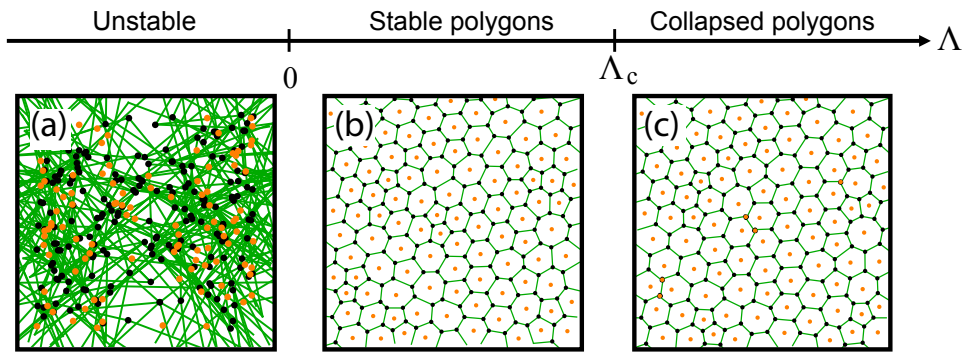

Figure 1. Confluent active foam model stability An analytic stability calculation for an active foam model of ordered confluent cellular tilings suggests that tilings should be stable for $0 < \Lambda < \Lambda_c$. Above Λ_c cells should collapse to zero area and below 0 the cell edge lengths should grow without bound. Panels (a-c) show snapshots from numerical simulations of disordered tilings in each of these scenarios. Although (b) and (c) look similar, (b) is a steady state while (c) is a snapshot from early in a simulation where cells will continue to shrink to zero area and the foam will coarsen indefinitely. At this timestep, there are just a few cells that have collapsed in the middle and the lower left-hand corner, as their centers – orange dots – are sitting on top of vertices.

This means that the confluent limit of the active foam model cannot access the fluid phase seen in standard vertex models, as any potential rigidity transition would happen for $\Lambda < 0$ where the model itself is unstable.

Spring Edge Model

We next discuss the spring edge model, where every edge is governed by its own linear spring of rest length l_0. First-order rigidity theory, also known as Maxwell constraint counting ***Damavandi et al.*** (***2022a***), suggests that the model should never be floppy: $N_{d.o.f.} = 4N_{cell}$, $N_{constraints} = M = N_{cell} + 3N_{cell} = 4N_{cell}$, therefore $N_{d.o.f.} = M$. A similar situation occurs in the 2D Voronoi model, as discussed by Sussman and Merkel ***Sussman and Merkel*** (***2018***), and also in fiber networks with bending moduli ***Shivers et al.*** (***2019***).

Even though such systems do not exhibit a singular rigidity transition, there is still a crossover from soft to stiff behavior. In the 2D Voronoi model, no rigidity transition is observed in the limit of zero temperature (activity), but in the presence of finite fluctuations there is a strong crossover from solid-like behavior to fluid-like behavior at a critical value of p_0 ***Sussman and Merkel*** (***2018***). Similarly, fiber network models with a bending energy are always rigid, but the network can be arbitrarily soft at small strains and connectivities, and the stiffness increases dramatically as the connectivity or strain increases past a critical value.

As highlighted in Figure 2, simulations at zero temperature confirm that Maxwell constraint counting is predictive for the spring edge model; all configurations have a finite shear modulus.

However, we observe that the system exhibits a crossover from very soft to stiff as the model parameter l_0 decreases. This crossover involves a change in cell shapes from more regular and convex to more irregular and concave. The crossover becomes sharper as K_A is decreased and in the limit of $K_A = 0$ it becomes a singular rigidity transition (Fig 2(a)), as has been observed previously for spring networks ***Merkel et al.*** (***2019***); ***Vermeulen et al.*** (***2017***); ***Shivers et al.*** (***2019***), and the drop in the magnitude of the modulus at the crossover for $K_A \neq 0$ scales with K_A, as highlighted in the inset to Fig 2(a). This is highly reminiscent of observations in spring networks with a bending energy, and suggests that the area term in the spring-edge model is playing the same role as the bending term in fiber networks.

These observations suggest that when the area compressibility K_A takes on small or intermediate values, the spring-edge model behaves similarly to the standard vertex model in the sense that there is a transition from a nearly floppy state with a low shear modulus to a stiff state with a high shear modulus as the cell interfaces become more stiff (e.g. l_0 decreases).

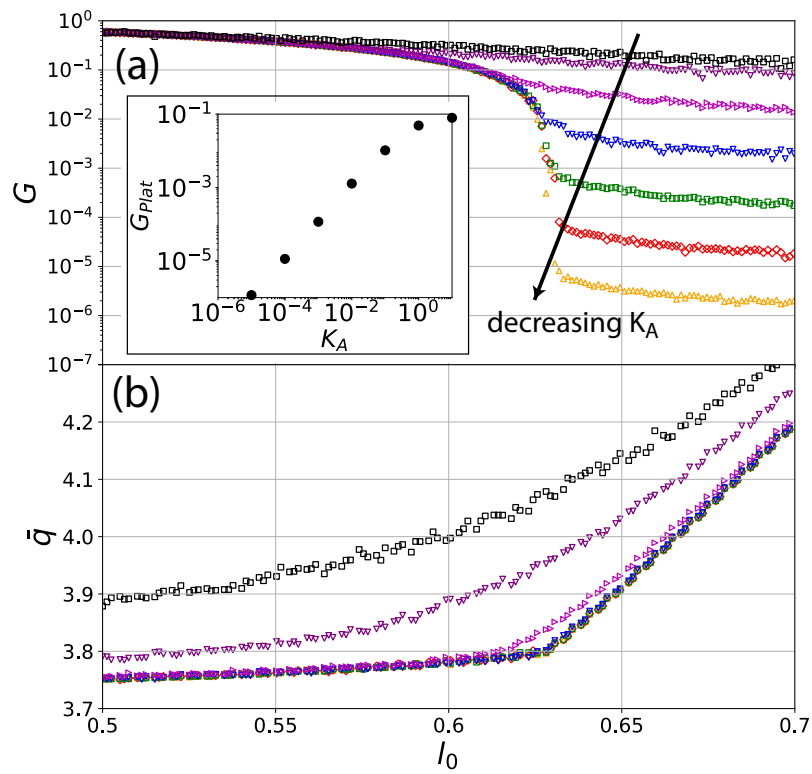

Figure 2. Rigidity in the Spring-Edge model (a) Shear modulus G as a function of spring rest length l_0 for different values of $K_A \in (1\times10^{-5}, 1\times10^{-4}, 1\times10^{-3}, 0.01, 0.1, 1, 10)$ in the Spring-Edge model. The inset is a plot of the plateau of the shear modulus G_{plat} in the floppy regime as a function of K_A. (b) Observed cell shape index as a function of l_0 for different values of K_A in the same range as in panel (a), highlighting that there is a large change in the behavior of that observable at the crossover point, very similar to what is seen in the standard vertex model.

Previous work on the standard vertex model highlights a strong connection between observed cell shape and the floppy-to-rigid transition, which is also observed in experiments ***Park et al.*** (***2015***); ***Wang et al.*** (***2020***). Therefore, an obvious question is whether there is a similar relationship in the spring-edge model. Fig 2(b) shows the observed 2D shape index $\bar{q}$ as a function of model parameter l_0 for different values of K_A. In the parameter regime where the tissue is stiff, $\bar{q}$ changes very little and is pinned near a characteristic value $\bar{q} *\sim 3.75$, while in the parameter regime where the tissue is nearly floppy, $\bar{q}$ rises quickly away from that characteristic value. Qualitatively, this

behavior is nearly identical to what is observed in standard vertex model simulations ***Park et al.*** (***2015***); ***Wang et al.*** (***2020***), and predicted by vertex model scaling arguments ***Merkel et al.*** (***2019***).

Taken together, this highlights that at least in some parameter regimes, the spring-edge model exhibits shape-tissue fluidity correlations that are remarkably similar to those in standard vertex models. This in turn suggests both that i) an observation of such a correlation in experimental data can not be used to distinguish between models and ii) a strong correlation between shape and tissue fluidity could potentially be a universal feature of a broad class of models.

Dynamical models

We are interested in understanding whether dynamical models also exhibit a rigidity transition in the limit of infinitely slow driving. To calculate the standard definition of the shear modulus in presence of zero fluctuations, a model must exhibit a force-balanced steady state in that quasi-static limit; otherwise, the steady state will be dynamic with timescales that compete with the shear driving rate, and the shear modulus is not well-defined.

In what follows, we distinguish between the vertex degrees of freedom $\{r_i\}$ (or equivalently, $\{A_\alpha, \{l_{ij}\}\}$) and the internal degrees of freedom, such as the rest lengths l_{ij}^0 and myosin density m_{ij} for the active tension model.

If a model's system of differential equations does possess a steady state where all the vertices $\{r_i\}$ remain at fixed positions that correspond to a local energy minimum, we term that a quasi-static steady state (QSS). Obviously many dynamical systems do not have such a state. Therefore, to see if such a state exists, we first construct nullclines of the dynamical model to identify possible steady states. Next, we attempt to construct a static vertex energy function (denoted by E^*) restricted to the steady state configurations, where, for example, the tensions in Eq 1 are no longer functions of time but only vertex coordinates. Finally, we analyze whether that static system defined by E^* exhibits a response to vertex perturbations that is equivalent to dynamics of the full dynamical system near that fixed point. If so, we have successfully identified a QSS with a well-defined shear modulus.

First, we argue that in the limit of fast vertex dynamics and slow internal DOF dynamics none of these dynamical models possess a QSS on disordered networks. To see this, assume that vertex relaxation happens at a fast rate, so that before internal states have changed much, vertices have reached mechanical equilibrium. This equilibrium generically involves a distribution of tensions for random packings. Thus at timescales when the internal dynamics start to become relevant, each rest length will change by a different rate based on the tension on the edge. This will break force balance and cause vertices to move again, negating the existence of a steady state. In other words, the fast vertex dynamics are always coupled to the slow internal rest length dynamics and a QSS is not achieved.

Of course the system can also achieve a steady state when the dynamics of both sets of degrees of freedom simultaneously reach their fixed points, but such a system will exhibit dynamics over finite timescales and also does not have a QSS. Therefore, in what follows we focus on the limit that the internal dynamics are fast compared to vertex degrees of freedom.

Active Spring Model

For the active spring model, first assume that $\epsilon_c = 0$. Then at steady state, $l_{ij}^{0*} = l_{ij}$ and $T_{ij}^* = 0$. Thus, the equivalent static energy E^* is given by

$$E^* = \sum_\alpha K_A (A_\alpha - A_0)^2.$$

More generally, for $\epsilon_c > 0$, some edges will still hold tensions but the maximum strain on an edge will be ϵ_c. In other words, for those edges with $|\epsilon_{ij}(t=0)| > \epsilon_c$ the steady state will be reached when

$|\epsilon_{ij}^*| = \epsilon_c$ or $l_{ij}^{0*} = l_{ij}/(1 \pm \epsilon_c)$:

$$l_{ij}^{0*} = \begin{cases} \frac{l_{ij}}{1+\epsilon_c} & \text{if } \epsilon_{ij} > \epsilon_c \\ l_0 & \text{if } -\epsilon_c \leq \epsilon_{ij} \leq \epsilon_c \\ \frac{l_{ij}}{1-\epsilon_c} & \text{if } \epsilon_{ij} < -\epsilon_c \end{cases} \tag{19}$$

where l_0 is the initial rest length of the whole system. The tension T^* at steady state is

$$T_{ij}^* \propto \begin{cases} \frac{\epsilon_c}{1+\epsilon_c} l_{ij} & \text{if } \epsilon_{ij} > \epsilon_c \\ (l_{ij} - l_0) & \text{if } -\epsilon_c \leq \epsilon_{ij} \leq \epsilon_c \\ \frac{-\epsilon_c}{1-\epsilon_c} l_{ij} & \text{if } \epsilon_{ij} < -\epsilon_c \end{cases} \tag{20}$$

To get the equivalent static energy E^*, we insert the tensions in Eq. 1 and integrate. The reason we should not use the spring edge energy function is because in this steady state system, rest length is a function of l_{ij} and so needs to be properly integrated.

Now, assume this equivalent static model has a stable fixed point. Does it have an equivalent dynamics to the actual dynamical system near the fixed point? In other words, if we perturb away from the fixed point $\mathbf{r}_i = \mathbf{r}_i^* + \delta\mathbf{r}_i$, is $\delta\mathbf{r}_i$ obtained from E^* the same as $\delta\mathbf{r}_i$ we get from the dynamical system? The answer should be yes if we are to claim E^* is an equivalent static representation of the dynamical model. Here for simplicity, we assume the pressure is uniform across the tissue (or equivalently, $K_A \approx 0$). Also, we assume that the edge strains $|\epsilon_{ij}| > \epsilon_c$ so that internal rest length dynamics has been activated (otherwise, the system would simply be a spring-edge model). Then, at equilibrium, $|\epsilon_{ij}^*| = \epsilon_c$.

First, some useful algebra: if $\mathbf{r}_i = \mathbf{r}_i^* + \delta\mathbf{r}_i$, then to first order, $\delta l_{ij} = \hat{\mathbf{r}}_{ij}^* \cdot \delta\mathbf{r}_{ij}$, the unit vector along edge l_{ij} is $\hat{\mathbf{r}}_{ij} = \hat{\mathbf{r}}_{ij}^* + \delta\hat{\mathbf{r}}_{ij} = (\mathbf{r}_{ij}^* + \delta\mathbf{r}_{ij})/(l_{ij}^* + \delta l_{ij}) = \hat{\mathbf{r}}_{ij}^* + \delta\mathbf{r}_{ij}^{\perp}/l_{ij}^*$ where $\delta\mathbf{r}_{ij}^{\perp} = \delta\mathbf{r}_{ij} - (\hat{\mathbf{r}}_{ij}^* \cdot \delta\mathbf{r}_{ij})\hat{\mathbf{r}}_{ij}^*$.

The vertex dynamics is given by $\dot{\mathbf{r}}_i = \mu\mathbf{F}_i = -\mu \sum_{\{j\}_i} K_l(l_{ij} - l_{ij}^0)\hat{\mathbf{r}}_{ij}$. At equilibrium, $\sum_{\{j\}_i}(l_{ij}^* - l_{ij}^{0*})\hat{\mathbf{r}}_{ij}^* = 0$. Then, for $\delta\mathbf{r}_i$ and δl_{ij}^0 we have

$$\delta\dot{\mathbf{r}}_i = -\mu K_l \sum_{\{j\}_i} \left(\frac{\pm\epsilon_c}{1 \pm \epsilon_c}\delta\mathbf{r}_{ij} + \frac{1}{1 \pm \epsilon_c}(\hat{\mathbf{r}}_{ij}^* \cdot \delta\mathbf{r}_{ij})\hat{\mathbf{r}}_{ij}^* - \delta l_{ij}^0 \hat{\mathbf{r}}_{ij}^* \right)$$

$$\delta\dot{l}_{ij}^0 = k\left(\frac{\pm\epsilon_c}{1 \pm \epsilon_c} l_{ij}^* + \hat{\mathbf{r}}_{ij}^* \cdot \delta\mathbf{r}_{ij} - \delta l_{ij}^0 \right)$$

δl_{ij}^0 is only nonzero for edges with strains $|\epsilon_{ij}| > \epsilon_c$ after the perturbation. If we assume that, with a fast rest length dynamics compared to vertex relaxation, we get $\delta l_{ij}^0 = 0$ when $|\epsilon_{ij}| = \epsilon_c$, or

$$(1 \pm \epsilon_c)\frac{\hat{\mathbf{r}}_{ij}^* \cdot \delta\mathbf{r}_{ij} - (1 \pm \epsilon_c)\delta l_{ij}^0}{l_{ij}^*} = 0. \tag{21}$$

The solution is $\hat{\mathbf{r}}_{ij}^* \cdot \delta\mathbf{r}_{ij} = (1 \pm \epsilon_c)\delta l_{ij}^0$. Plugging this back into the vertex relaxation dynamics, we get

$$\delta\dot{\mathbf{r}}_i = -\mu K_l \sum_{\{j\}_i} \frac{\pm\epsilon_c}{1 \pm \epsilon_c}\delta\mathbf{r}_{ij}. \tag{22}$$

Now, let's start from the equivalent static model. The tension is $T_{ij}^* = \pm\epsilon_c l_{ij}^*/(1 \pm \epsilon_c)$. So

$$\dot{\mathbf{r}}_i = -\mu K_l \sum_{\{j\}_i} \frac{\pm\epsilon_c l_{ij}}{(1 \pm \epsilon_c)} l_{ij}\hat{\mathbf{r}}_{ij} \tag{23}$$

$$\rightarrow \delta\dot{\mathbf{r}}_i = -\mu K_l \sum_{\{j\}_i} \frac{\pm\epsilon_c}{1 \pm \epsilon_c}\delta\mathbf{r}_{ij}, \tag{24}$$

which is the same as the actual dynamical system. However, recall that Eq. 22 is only correct if $|\epsilon_{ij}| > \epsilon_c$, but that is not guaranteed generically. Almost surely, vertex perturbations will lead to

some strains $|\epsilon_{ij}| < \epsilon_c$ in which case internal dynamics for those edges will not be activated and E^* will not generate dynamics equivalent to dynamical model. Only when $\epsilon_c = 0$ is the linear response to perturbations of coordinates for E^* equivalent to the dynamical model in the QSS limit. This is an uninteresting case since all edges will have zero strains and the model is floppy.

To confirm these analytic results, we have simulated the equivalent static model on random vertex networks and demonstrated that the energy function given by the tensions in Eq. 20 typically do not have a stable fixed point except in the limit of $\epsilon_c = 0$.

Tension Remodeling Model

For the tension remodeling model, assume that we start with uniform tension $T_{ij}(t=0) = \Lambda$ on all edges. At steady state, $l_{ij}^{0*} = l_{ij}$. If $|\epsilon_{ij}(t=0)| > \epsilon_c$, we have $\dot{T}_{ij} = -k_{e,c}/k_l \dot{l}_{ij}^0$. Integrating this gives

$$T_{ij}^* - \Lambda = \frac{-k_{e,c}}{k_l}\left(l_{ij}^0(|\epsilon_{ij}| = \epsilon_c) - l_0\right),$$

which leads to

$$T_{ij}^* = \begin{cases} \Lambda - \frac{k_e}{k_l}\left(\frac{l_{ij}}{1+\epsilon_c} - l_0\right) & \text{if } \epsilon_{ij} > \epsilon_c, \\ \Lambda & \text{if } -\epsilon_c \le \epsilon_{ij} \le \epsilon_c, \\ \Lambda - \frac{k_c}{k_l}\left(\frac{l_{ij}}{1-\epsilon_c} - l_0\right) & \text{if } \epsilon_{ij} < -\epsilon_c. \end{cases} \tag{25}$$

The tension can now show spring-like behavior. As before, integrating Eq. 1 with T_{ij}^* gives us the equivalent static model energy, E^*.

We will follow the same procedure as the active spring model to see if the equivalent static model is equivalent to the QSS limit of the dynamical model in the limit of fast internal dynamics. Using force balance at equilibrium, $\sum_{\{j\}_i} T_{ij}^* \hat{\mathbf{r}}_{ij}^* = 0$, we find

$$\delta\dot{\mathbf{r}}_i = -\mu \sum_{\{j\}_i} T_{ij}^* \left(\frac{\delta\mathbf{r}_{ij}}{l_{ij}^*} - \frac{1}{l_{ij}^*}\hat{\mathbf{r}}_{ij}^*(\hat{\mathbf{r}}_{ij}^* \cdot \delta r_{ij})\right) + \delta T_{ij}\hat{\mathbf{r}}_{ij}^*. \tag{26}$$

Here we assume that initially $|\epsilon_{ij}| > \epsilon_c$ so that the internal dynamics has been activated and $T_{ij}^* = \Lambda - k'(\frac{l_{ij}^*}{1\pm\epsilon_c} - l_0)$ where $k' = k_{e,c}/k_l$. Furthermore, we assume that the perturbation $\dot{\mathbf{r}}_i$ has led to $|\epsilon_{ij}| > \epsilon_c$ again so that $\delta T_{ij} \neq 0$. From Eqs. 11 and 12 we can see

$$\delta\dot{T}_{ij} = -k'\delta\dot{l}_{ij}^0$$
$$\rightarrow \delta T_{ij} = -k'\delta l_{ij}^0.$$

Note that $\delta T_{ij}(t=0) = 0$ and $\delta l_{ij}^0(t=0) = 0$. From Eq. 11, $\delta\dot{T}_{ij} = 0$ and QSS is achieved when $|\epsilon_{ij}| = \epsilon_c$ or $\hat{\mathbf{r}}_{ij}^* \cdot \delta\mathbf{r}_{ij} = (1 \pm \epsilon_c)\delta l_{ij}^0$ (Eq. 21). Thus at QSS we get $\delta T_{ij} = \hat{\mathbf{r}}_{ij}^* \cdot \delta\mathbf{r}_{ij}/(1 \pm \epsilon_c)$ and

$$\delta\dot{\mathbf{r}}_i = -\mu \sum_{\{j\}_i} (\Lambda + k' l_0)\frac{\delta\mathbf{r}_{ij}^\perp}{l_{ij}^*} - \frac{k'}{1 \pm \epsilon_c}\delta\mathbf{r}_{ij}. \tag{27}$$

If we start with the equivalent static system, it is easy to see that we get the same vertex relaxation dynamics. However, again this is only true if $|\epsilon_{ij}| > \epsilon_c$ for all edges after a perturbation, which is not generically the case. So, similarly to active spring model, tension remodeling only has an equivalent QSS in the limit of $\epsilon_c = 0$. Even then, the equivalent static model does not have a stable fixed point in simulations, which can be predicted from Eq. 25: the spring strains on the edges have the wrong sign and do not act as restoring forces.

In summary, both the active spring and tension remodeling models do not possess a quasi-static steady state except in the limit of $\epsilon_c = 0$, where the system is trivial and the network is floppy. Therefore, it is not possible to calculate a shear modulus independent of the applied shear rate for these models, and they are clearly distinct from the standard vertex model in the limit of slow shear.

Active Tension Network

For the active tension model, at steady state the tension is dictated by the myosin distribution: $T^*_{ij} = m^*_{ij}$. Moreover, from Eq. 16, $\dot{\ln}(m_{ij}) = \alpha \dot{\ln}(l^0_{ij})$ so that

$$m^*_{ij} = m_0 \left(\frac{l^{0*}_{ij}}{l_o} \right)^{\alpha} \tag{28}$$

where we have assumed that a uniform myosin field m_0 at $t = 0$. If we further assume $l^{0*}_{ij} = l_0 + \epsilon l_0$ such that $|\epsilon| \ll 1$ we can simplify Eq. 28 to read

$$m^*_{ij} \approx m_0 \left(1 + \alpha \frac{l^{0*}_{ij} - l_0}{l_0} \right). \tag{29}$$

From $T^*_{ij} = K_l(l_{ij} - l^{0*}_{ij}) = m^*_{ij}$ we can then describe l^{0*}_{ij} in terms of l_{ij}.

$$l^{0*}_{ij} \approx \frac{l_0 \left(l_{ij} - \frac{m_0 - \alpha m_0}{K_l} \right)}{l_0 + \frac{m_0 \alpha}{K_l}} \tag{30}$$

Finally, the tension is given by

$$T^*_{ij} \approx \frac{m_0 \left(l_0 + \alpha(l_{ij} - l_0) \right)}{l_0 + \frac{m_0 \alpha}{K_l}} \tag{31}$$

which, similar to the previous models, exhibits spring-like behavior. In fact, we can rewrite Eq. 31 as

$$T^*_{ij} \approx \tilde{K}_l (l_{ij} - \tilde{l}_0), \tag{32}$$

where the effective rest length is

$$\tilde{l}_0 = l_0 - \frac{l_0}{\alpha}, \tag{33}$$

and the effective spring constant is

$$\tilde{K}_l = \frac{\alpha K_l m_0}{K_l l_0 + \alpha m_0}. \tag{34}$$

This equation indicates that the two myosin activity parameters m_0 and α allow the effective rest length and effective spring constant to be independently varied.

Finally, we compare the behavior of the equivalent static energy functional perturbed from its minimum energy to the actual dynamical system near its fixed point. First, we focus on the equivalent static system. Starting from the tension given by Eq. 31, we can find δT_{ij} for the ES model in response to perturbation $\delta \mathbf{r}_i$:

$$\delta T_{ij} = \frac{K_l m_0 \alpha}{m_0 \alpha + K_l l_0} \delta l_{ij} = \frac{K_l m_0 \alpha}{m_0 \alpha + K_l l_0} \delta \mathbf{r}_{ij} \cdot \hat{\mathbf{r}}^*_{ij} \tag{35}$$

Now, we study the actual dynamical model. Vertex relaxation after perturbation is given by Eq. 26. We need to find δT_{ij} at QSS for comparison. To do so, we first write the δl^0_{ij} and δm_{ij} dynamics:

$$\begin{aligned} \frac{1}{l^{0*}_{ij}} \delta l^0_{ij} &= \tau_l^{-1} \frac{\delta T_{ij} - \delta m_{ij}}{m^*_{ij}} \\ \frac{1}{m^*_{ij}} \delta m_{ij} &= \alpha \tau_l^{-1} \frac{\delta T_{ij} - \delta m_{ij}}{m^*_{ij}} \end{aligned} \tag{36}$$

In the limit of fast internal dynamics then, we have $\delta T_{ij} = \delta m_{ij}$. From Eq. 16 we also have

$$\frac{m_{ij}}{m_0} = \left(\frac{l^0_{ij}}{l_o} \right)^{\alpha}.$$

Assuming $(l_{ij}^0 - l_0)/l_0 \ll l_0$ and using the fact that at equilibrium $T_{ij}^* = m_{ij}^*$ and $\delta T_{ij} = \delta m_{ij}$, we find

$$\frac{T_{ij}^* + \delta T_{ij}}{m_0} = 1 + \alpha \frac{l_{ij}^{0*} + \delta l_{ij}^0 - l_0}{l_0}$$
$$\rightarrow \delta l_{ij}^0 = \frac{l_0}{m_0 \alpha} \delta T_{ij}.$$

Since T_{ij} is the tension of a spring, we have

$$\delta T_{ij} = K_l(\delta l_{ij} - \delta l_{ij}^0) = K_l(\delta \mathbf{r}_{ij} \cdot \hat{\mathbf{r}}_{ij}^* - \frac{l_0}{m_o \alpha} \delta T_{ij}) \tag{37}$$

$$\rightarrow \delta T_{ij} = \frac{K_l m_0 \alpha}{m_0 \alpha + K_l l_0} \delta \mathbf{r}_{ij} \cdot \hat{\mathbf{r}}_{ij}^* \tag{38}$$

which is the same as δT_{ij} given from the effective static model, Eq. 35. Therefore, we can conclude that unlike the other two dynamical models, the active tension network matches the equivalent static model in the limit of fast internal dynamics. Moreover, we have confirmed in numerical simulations that a system with tensions given by Eq. 31 is indeed able to find a stable energy minimum.

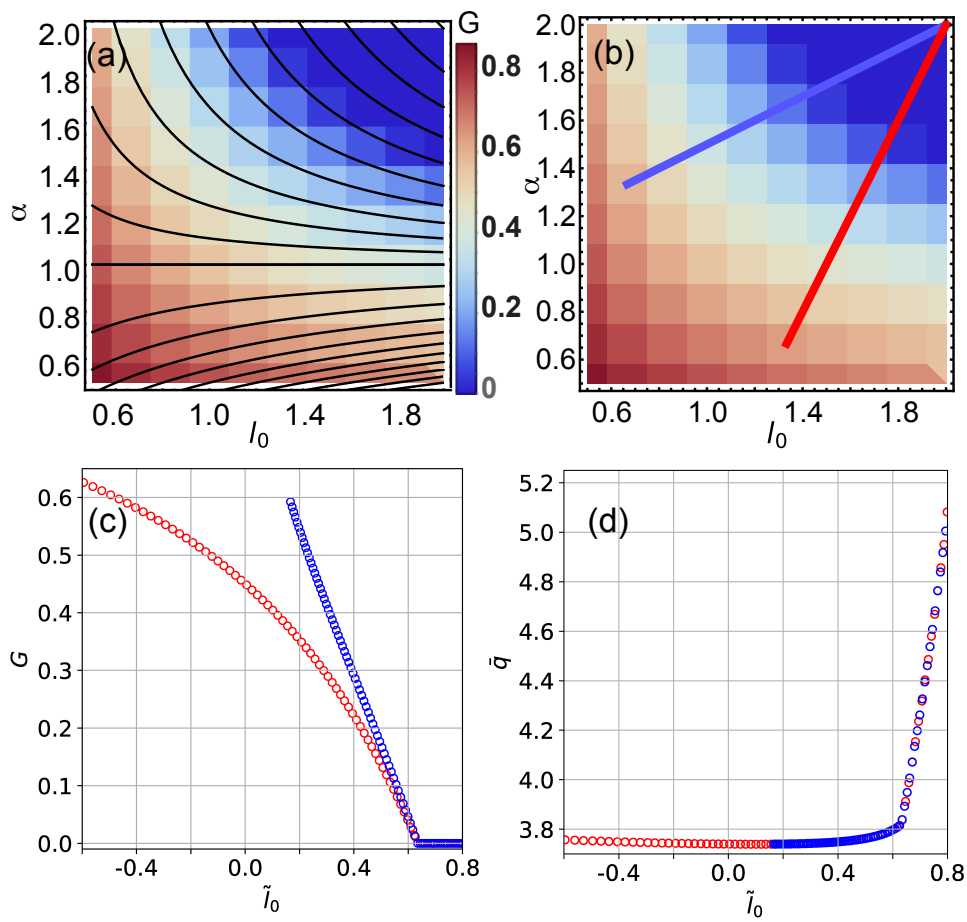

Figure 3. Quasi-static linear response of the Active tension model (a) Shear modulus of the quasi-static active tension model as a function of myosin recruitment rate α and spring rest length l_0. Contours illustrate lines of constant $\tilde{l}_0$. (b) Same plot as figure (a), where red and blue lines illustrate two trajectories with linearly increasing effective rest length $\tilde{l}_0$. (c) Shear modulus as a function of effective spring rest length $\tilde{l}_0$ for two different trajectories through model space, illustrated by the red and blue lines in panel (b). (d) Observed shape index $\bar{q}$ as a function of effective spring rest length $\tilde{l}_0$ for two different trajectories, illustrating a strong crossover in shape at the location of the floppy-to-rigid transition.

Next, we calculate the shear modulus in simulations of this vertex model. Here we present data for $K_A = 0.0$, but the data is quite similar for small $K_A > 0.0$. Fig 3(a) illustrates the ensemble-averaged shear modulus G as a function of the model parameters l_0 and α. The contours illustrate lines of constant $\tilde{l}_0$. For example, at $\alpha = 1.0$, $\tilde{l}_0 = 0$ for any l_0. Above this line corresponds to $\tilde{l}_0 > 0$ while below is $\tilde{l}_0 < 0$. For large values of the spring rest length and myosin recruitment rate, the shear modulus is zero and the system is floppy, while for lower values of these parameters the system becomes rigid.

To understand the origin of this behavior, we study the linear response along lines of linearly increasing effective rest length $\tilde{l}_0$ (Eq. 33), illustrated by the blue and red lines in Fig 3(b). Fig 3(c) demonstrates that as a function of the effective rest length, the active tension network is quite similar to the spring-edge model, with a shear modulus that is zero above a critical value of the effective rest length $\tilde{l}_0 > l_0^c$.

Importantly, the extra model parameter α generates extra flexibility in the model, modulating the effective spring constant. Therefore, although the rigidity transition always occurs at the same value of the effective spring constant, the stiffness of the system once it becomes rigid can be independently regulated. Additionally, the model can exhibit $\tilde{l}_0 < 0$, which normally would be unphysical for a spring network but here it can be achieved with $l_0 > 0$ and $\alpha < 1$. This also allows the system to become stiffer than in a simple spring-edge model.

Fig 3(d) shows the observed cell shape index $\overline{q}$ as a function of $\tilde{l}_0$ for the same two trajectories in parameter space highlighted in panel Fig 3(b). Importantly, the shape parameter shows the same behavior as all other variations of the vertex model with a well-defined shear modulus that we have studied: $\overline{q}$ remains pinned at a low value of 3.75 in the stiff/rigid phase of the model, and rises sharply away from that value in the floppy regime.

Discussion and Conclusions

We have studied the rigidity transition in six different variations on the vertex model for confluent tissues. We find that a subset of them – the spring-edge model and the active tension network – exhibit a crossover from floppy to stiff at a characteristic value of a model parameter: the effective spring rest length, accompanied by an abrupt change in the behavior of the observed cell shape, when K_A is small. This suggests that there may be a broad class of energy functionals (some even with extra dynamics) that all generate the same universal features.

In contrast, we find that the confluent foam model is numerically unstable in the regime that would be floppy, and so there is no floppy-to-rigid or fluid-to-solid transition in that model. This highlights that the confluent foam model may not be able to recapitulate the fluid-like behavior has been observed in multiple confluent epithelial systems ***Wang et al.*** (***2020***); ***Park et al.*** (***2015***).

We also find that the dynamics in the active spring and tension remodeling models do not permit a well-defined quasi-static limit. We demonstrate that the steady states of such systems necessarily involve remodeling of the tension network on timescales that would compete with taking the limit of zero strain rate to compute the shear modulus, and so it is not possible to simulate or analyze the models in such a limit. This highlights that these models can not exhibit the universal features for the shear modulus identified in the standard vertex model.

To avoid arbitrary thresholds and make initial progress, here we used the shear modulus to define rigidity. An interesting future direction is to investigate the behavior of these models at finite strain rates or with finite levels of fluctuations. For example, it should be possible to apply oscillatory shear strain to these models with a finite frequency and quantify the nonlinear rheology of these models (e.g. the storage and loss modulus) as a function of frequency.

In previous work, it was shown that the 2D Voronoi model is marginally rigid even to first-order (i.e. based on Maxwell constraint counting) and therefore the shear modulus is always be finite ***Sussman and Merkel*** (***2018***). However, in the presence of finite fluctuations the 2D Voronoi model still exhibits a crossover from nearly floppy to quite stiff as a function of the target shape

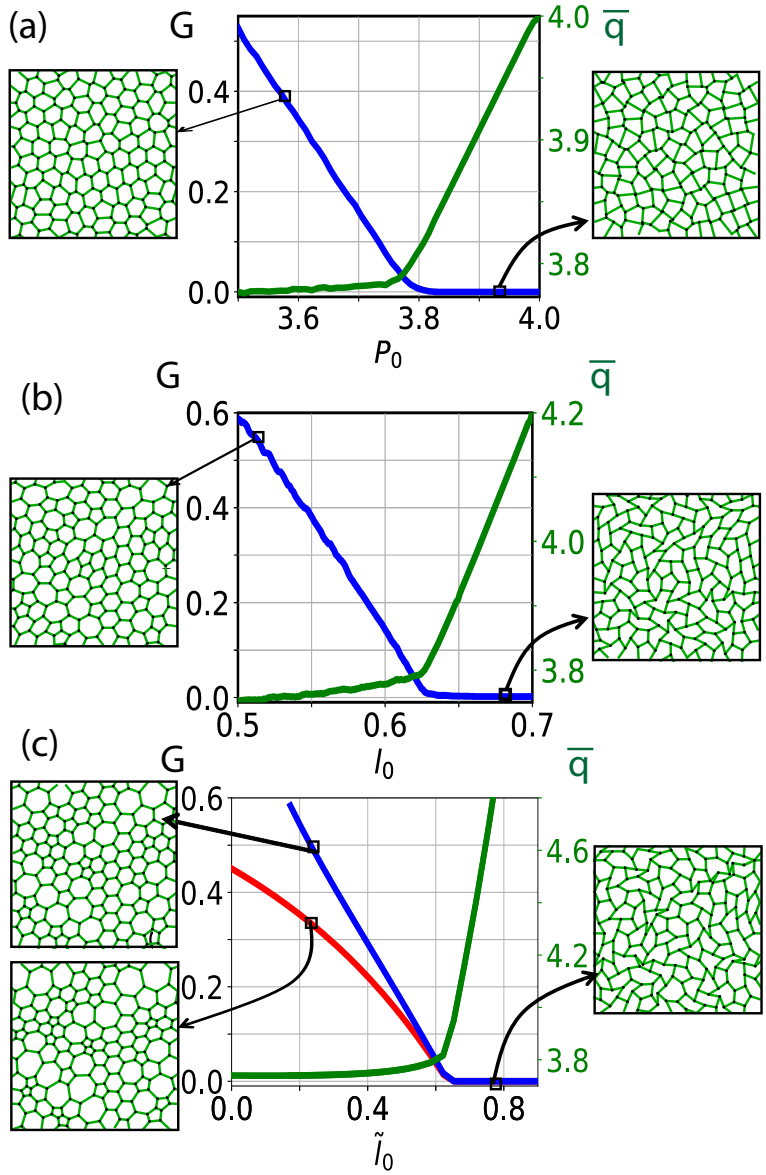

Figure 4. Schematic diagram of universal behavior in vertex models. All three models, the (a) Standard vertex model, the (b) Spring-Edge model, and the (c) Active tension model exhibit a crossover from soft (low shear modulus G) to stiff (high shear modulus) behavior as a function of the control parameter, with an associated change in observed cell shape $\bar{q}$.

index, and that this crossover happens at roughly the same value of the shape index found in the 2D vertex model. Therefore, it is interesting to speculate that something similar could occur in the active spring and tension remodeling models – although they do not have a well-defined quasi-static limit, perhaps they exhibit a crossover in stiffness at low driving frequencies. Or, it could be that there is no hint of such a transition and the behavior is simply non-universal.

Another important point is that our argument that there are no quasi-static steady states in dynamical models where the vertex degrees of freedom are fast compared to the internal degrees of freedom relies on the fact that forces do not generically balance in networks with random tensions. In other words, such states are a set of measure zero in the configuration space. However, this argument may break down in ordered lattices (with crystalline geometries), and it is also possible that mechanosensitive cell behaviors could drive a tissue towards such non-generic states. Inves-

tigating whether plausible local feedback rules could generate quasi-static solid states is another potential avenue for future work.

Interestingly, the extra myosin degrees of freedom introduced in the active tension network (which were needed to match experimental observations) give that model a higher degree of tunability than the standard vertex model. Simply by tuning the myosin recruitment parameter α, the tissue is able to tune its collective overall stiffness, which could be functionally beneficial in developing embryos. It would be interesting to investigate how various fruit fly mutations alter this parameter and study whether the observations of global embryo shape and dynamics are consistent with changing overall stiffness.

Perhaps the most intriguing result of this work is that the observed cell shape index is an excellent predictor for the onset of rigidity/stiffening in all of the models that have a well-defined shear modulus. This is surprising, as the control parameter in both the spring-edge and active tension models is not the shape, but the spring rest length. Our demonstration that observed cell shape index predicts rigidity in a variety of reasonable mechanical models for cells helps to explain why it has been so successful and useful in experiments. However, this is an observation that raises new questions. Why is it universal?

One hint is provided by recent work that indicates a geometric incompatibility ***Merkel et al.*** (***2019***); ***Moshe et al.*** (***2018***) is driving a second-order rigidity transition in the standard vertex model, and that the same mechanism drives strain-stiffening in fiber networks ***Damavandi et al.*** (***2022a***). These works highlight that there are two length scales in the system: 1) one defined by the number of cells/vertices per unit area and 2) the characteristic distance between two cells or vertices defined by the energy functional (parameterized by the cell perimeter in vertex models or the rest length for edges in spring-edge models). Rigidity occurs when the second, energy-defined length scale becomes smaller than the first, density-based length scale. In the rigid phase, there appear to be no states with the specified density that allow the system to have zero energy, and the second-order rigidity transition occurs at a special point in configuration space where energy-density compatible states disappear. Given that we think this second-order rigidity transition is universal in all these models, it could be that the observed cell shape index, which is one of the obvious dimensionless numbers that compares those two length scales, is a good order parameter for the transition across all types of models for tissues. More work is needed to understand whether many (or all) second-order rigidity transitions share these universal geometric features, which could allow us to make these ideas quantitatively precise.

Acknowledgements

We acknowledge support from the Simons Foundation grants No 454947 to MLM (OKD and MLM) and No 446222 (MLM and ELK), and MLM acknowledges support from NSF-DMR-1951921.

References

Angelini TE, Hannezo E, Trepatc X, Marquez M, Fredberg JJ, Weitz DA. Glass-like dynamics of collective cell migration. Proceedings of the National Academy of Sciences of the United States of America. 2011; 108(12):4714–4719. doi: 10.1073/pnas.1010059108.

Ashcroft NW, Mermin ND. Solid State Physics. Holt-Saunders; 1976.

Basan M, Prost J, Joanny JF, Elgeti J. Dissipative particle dynamics simulations for biological tissues: rheology and competition. Physical Biology. 2011 Apr; 8(2):026014. https://iopscience.iop.org/article/10.1088/1478-3975/8/2/026014, doi: 10.1088/1478-3975/8/2/026014.

Bi D, Lopez JH, Schwarz JM, Manning ML. A density-independent rigidity transition in biological tissues. Nature Physics. 2015; 11(12):1074–1079. doi: 10.1038/nphys3471.

Bi D, Yang X, Marchetti MC, Manning ML. Motility-driven glass and jamming transitions in biological tissues. Physical Review X. 2016; 6(2):1–13. doi: 10.1103/PhysRevX.6.021011.

Clément R, Dehapiot B, Collinet C, Lecuit T, Lenne PF. Viscoelastic dissipation stabilizes cell shape changes during tissue morphogenesis. Current biology. 2017; 27(20):3132–3142.

Damavandi OK, Hagh VF, Santangelo CD, Manning ML. Energetic rigidity. I. A unifying theory of mechanical stability. Physical Review E. 2022 Feb; 105(2):025003. https://link.aps.org/doi/10.1103/PhysRevE.105.025003, doi: 10.1103/PhysRevE.105.025003.

Damavandi OK, Hagh VF, Santangelo CD, Manning ML. Energetic rigidity. II. Applications in examples of biological and underconstrained materials. Physical Review E. 2022 Feb; 105(2):025004. https://link.aps.org/doi/10.1103/PhysRevE.105.025004, doi: 10.1103/PhysRevE.105.025004.

Das A, Sastry S, Bi D. Controlled Neighbor Exchanges Drive Glassy Behavior, Intermittency, and Cell Streaming in Epithelial Tissues. Physical Review X. 2021 Nov; 11(4):041037. https://link.aps.org/doi/10.1103/PhysRevX.11.041037, doi: 10.1103/PhysRevX.11.041037.

Devany J, Sussman DM, Manning ML, Gardel ML. Cell division Rate Controls Cell Shape Remodeling in Epithelia Department of Physics , James Franck Institute and Institute for Biophysical Dynamics , The University of Chicago , Chicago , IL 60637 , USA , 2 Department of Physics and Soft Matter. bioRxiv. 2019; .

Devany J, Sussman DM, Yamamoto T, Manning ML, Gardel ML. Cell cycle–dependent active stress drives epithelia remodeling. Proceedings of the National Academy of Sciences. 2021 Mar; 118(10):e1917853118. https://pnas.org/doi/full/10.1073/pnas.1917853118, doi: 10.1073/pnas.1917853118.

Duclut C, Paijmans J, Inamdar MM, Modes CD, Jülicher F. Nonlinear rheology of cellular networks. arXiv:210316462 [cond-mat, physics:physics]. 2021 Mar; http://arxiv.org/abs/2103.16462, arXiv: 2103.16462.

Erdemci-Tandogan G, Manning ML. Effect of cellular rearrangement time delays on the rheology of vertex models for confluent tissues. PLOS Computational Biology. 2021 Jun; 17(6):e1009049. https://dx.plos.org/10.1371/journal.pcbi.1009049, doi: 10.1371/journal.pcbi.1009049.

Farhadifar R, Röper JC, Aigouy B, Eaton S, Jülicher F. The Influence of Cell Mechanics, Cell-Cell Interactions, and Proliferation on Epithelial Packing. Current Biology. 2007 Dec; 17(24):2095–2104. https://linkinghub.elsevier.com/retrieve/pii/S0960982207023342, doi: 10.1016/j.cub.2007.11.049.

Grosser S, Lippoldt J, Oswald L, Merkel M, Sussman DM, Renner F, Gottheil P, Morawetz EW, Fuhs T, Xie X, Pawlizak S, Fritsch AW, Wolf B, Horn LC, Briest S, Aktas B, Manning ML, Käs JA. Cell and Nucleus Shape as an Indicator of Tissue Fluidity in Carcinoma. Physical Review X. 2021 Feb; 11(1):011033. https://link.aps.org/doi/10.1103/PhysRevX.11.011033, doi: 10.1103/PhysRevX.11.011033.

Hufnagel L, Teleman AA, Rouault H, Cohen SM, Shraiman BI. On the mechanism of wing size determination in fly development. Proceedings of the National Academy of Sciences. 2007 Mar; 104(10):3835–3840. https://pnas.org/doi/full/10.1073/pnas.0607134104, doi: 10.1073/pnas.0607134104.

Ilina O, Gritsenko PG, Syga S, Lippoldt J, La Porta CAM, Chepizhko O, Grosser S, Vullings M, Bakker GJ, Starruß J, Bult P, Zapperi S, Käs JA, Deutsch A, Friedl P. Cell–cell adhesion and 3D matrix confinement determine jamming transitions in breast cancer invasion. Nature Cell Biology. 2020; 22(9):1103–1115. http://dx.doi.org/10.1038/s41556-020-0552-6, doi: 10.1038/s41556-020-0552-6, publisher: Springer US.

Kim S, Pochitaloff M, Georgina-Stooke-Vaughan, Campàs O. Embryonic Tissues as Active Foams. bioRxiv. 2020; p. 2020.06.17.157909–2020.06.17.157909. https://www.biorxiv.org/content/10.1101/2020.06.17.157909v1, doi: 10.1101/2020.06.17.157909.

Latorre E, Kale S, Casares L, Gómez-González M, Uroz M, Valon L, Nair RV, Garreta E, Montserrat N, del Campo A, Ladoux B, Arroyo M, Trepat X. Active superelasticity in three-dimensional epithelia of controlled shape. Nature. 2018 Nov; 563(7730):203–208. http://www.nature.com/articles/s41586-018-0671-4, doi: 10.1038/s41586-018-0671-4.

Lawson-Keister E, Manning ML. Jamming and arrest of cell motion in biological tissues. Current Opinion in Cell Biology. 2021 Oct; 72:146–155. https://linkinghub.elsevier.com/retrieve/pii/S095506742100096X, doi: 10.1016/j.ceb.2021.07.011.

Li X, Das A, Bi D. Mechanical Heterogeneity in Tissues Promotes Rigidity and Controls Cellular Invasion. Physical Review Letters. 2019; 123(5):58101–58101. https://doi.org/10.1103/PhysRevLett.123.058101, doi: 10.1103/PhysRevLett.123.058101, publisher: American Physical Society.

Maxwell JC. L. On the calculation of the equilibrium and stiffness of frames. The London, Edinburgh, and Dublin Philosophical Magazine and Journal of Science. 1864 Apr; 27(182):294–299. https://doi.org/10.1080/14786446408643668, doi: 10.1080/14786446408643668, publisher: Taylor & Francis.

Merkel M, Baumgarten K, Tighe BP, Manning ML. A minimal-length approach unifies rigidity in underconstrained materials. Proceedings of the National Academy of Sciences of the United States of America. 2019; 116(14):6560–6568. doi: 10.1073/pnas.1815436116.

Merkel M, Manning ML. A geometrically controlled rigidity transition in a model for confluent 3D tissues. New Journal of Physics. 2018; 20(2). doi: 10.1088/1367-2630/aaaa13, publisher: IOP Publishing.

Mongera A, Rowghanian P, Gustafson HJ, Shelton E, Kealhofer DA, Carn EK, Serwane F, Lucio AA, Giammona J, Campàs O. A fluid-to-solid jamming transition underlies vertebrate body axis elongation. Nature. 2018; 561(7723):401–405. http://dx.doi.org/10.1038/s41586-018-0479-2, doi: 10.1038/s41586-018-0479-2, publisher: Springer US.

Moshe M, Bowick MJ, Marchetti MC. Geometric Frustration and Solid-Solid Transitions in Model 2D Tissue. Physical Review Letters. 2018; 120(26):268105–268105. https://doi.org/10.1103/PhysRevLett.120.268105, doi: 10.1103/PhysRevLett.120.268105, publisher: American Physical Society.

Nagai T, Honda H. A dynamic cell model for the formation of epithelial tissues. Philosophical Magazine B. 2001 Jul; 81(7):699–719. https://www.tandfonline.com/doi/full/10.1080/13642810108205772, doi: 10.1080/13642810108205772.

Noll N, Mani M, Heemskerk I, Streichan SJ, Shraiman BI. Active tension network model suggests an exotic mechanical state realized in epithelial tissues. Nature Physics. 2017; 13(12):1221–1226. doi: 10.1038/nphys4219.

Paoluzzi M, Angelani L, Gosti G, Marchetti MC, Pagonabarraga I, Ruocco G. Alignment interactions drive structural transitions in biological tissues. Physical Review E. 2021 Oct; 104(4):044606. http://arxiv.org/abs/2107.00523, doi: 10.1103/PhysRevE.104.044606, arXiv: 2107.00523.

Park JA, Kim JH, Bi D, Mitchel JA, Qazvini NT, Tantisira K, Park CY, McGill M, Kim SH, Gweon B, Notbohm J, Steward R, Burger S, Randell SH, Kho AT, Tambe DT, Hardin C, Shore SA, Israel E, Weitz DA, et al. Unjamming and cell shape in the asthmatic airway epithelium. Nature Materials. 2015; 14(10):1040–1048. doi: 10.1038/nmat4357.

Petridou NI, Corminas-Murtra B, Heisenberg CP, Hannezo E. Rigidity percolation uncovers the structural basis of embryonic tissue phase transitions. Accepted to Cell. 2021; .

Popović M, Druelle V, Dye NA, Jülicher F, Wyart M. Inferring the flow properties of epithelial tissues from their geometry. New Journal of Physics. 2021 Mar; 23(3):033004. https://iopscience.iop.org/article/10.1088/1367-2630/abcbc7, doi: 10.1088/1367-2630/abcbc7.

Sadhukhan S, Nandi SK. The origin of universal cell shape variability in a confluent epithelial monolayer. Biophysics; 2021.

Sanematsu PC, Erdemci-Tandogan G, Patel H, Retzlaff EM, Amack JD, Manning ML. 3D viscoelastic drag forces contribute to cell shape changes during organogenesis in the zebrafish embryo. Cells & Development. 2021 Jul; p. 203718. https://linkinghub.elsevier.com/retrieve/pii/S2667290121000528, doi: 10.1016/j.cdev.2021.203718.

Shivers JL, Arzash S, Sharma A, MacKintosh FC. Scaling Theory for Mechanical Critical Behavior in Fiber Networks. Physical Review Letters. 2019 May; 122(18):188003. https://link.aps.org/doi/10.1103/PhysRevLett.122.188003, doi: 10.1103/PhysRevLett.122.188003.

Staddon MF, Cavanaugh KE, Munro EM, Gardel ML, Banerjee S. Mechanosensitive Junction Remodeling Promotes Robust Epithelial Morphogenesis. Biophysical Journal. 2019; 117(9):1739–1750. https://doi.org/10.1016/j.bpj.2019.09.027, doi: 10.1016/j.bpj.2019.09.027, publisher: Biophysical Society.

Staple DB, Farhadifar R, Röper JC, Aigouy B, Eaton S, Jülicher F. Mechanics and remodelling of cell packings in epithelia. European Physical Journal E. 2010; 33(2):117–127. doi: 10.1140/epje/i2010-10677-0.

Sussman DM, Merkel M. No unjamming transition in a Voronoi model of biological tissue. Soft Matter. 2018; 14(17):3397–3403. doi: 10.1039/c7sm02127e, publisher: Royal Society of Chemistry.

Vermeulen MFJ, Bose A, Storm C, Ellenbroek WG. Geometry and the onset of rigidity in a disordered network. Physical Review E. 2017 Nov; 96(5):053003. https://link.aps.org/doi/10.1103/PhysRevE.96.053003, doi: 10.1103/PhysRevE.96.053003.

Wang X, Merkel M, Sutter LB, Erdemci-Tandogan G, Manning ML, Kasza KE. Anisotropy links cell shapes to tissue flow during convergent extension. Proceedings of the National Academy of Sciences of the United States of America. 2020; 117(24):13541–13551. doi: 10.1073/pnas.1916418117.

Weeks ER, Crocker JC, Levitt AC, Schofield A, Weitz DA. Three-Dimensional Direct Imaging of Structural Relaxation Near the Colloidal Glass Transition. Science. 2000 Jan; 287(5453):627–631. https://www.science.org/doi/10.1126/science.287.5453.627, doi: 10.1126/science.287.5453.627.

Yan L, Bi D. Multicellular Rosettes Drive Fluid-solid Transition in Epithelial Tissues. Physical Review X. 2019; 9(1):11029–11029. https://doi.org/10.1103/PhysRevX.9.011029, doi: 10.1103/PhysRevX.9.011029, publisher: American Physical Society.